Proceedings of the ASME 2024 19th International Manufacturing Science and Engineering Conference
MSEC2024
June 17 – June 21, 2024, Knoxville, Tennessee

MSEC2024-124538

PYRAMID LEARNING BASED PART-TO-PART CONSISTENCY ANALYSIS IN LASER POWDER BED FUSION

Erfan Ziad[1], Feng Ju[1], Zhuo Yang[2], Yan Lu[2]

[1]School of Computing and Augmented Intelligence, Arizona State University, Tempe, AZ
[2]Engineering Lab, National Institute of Standards and Technology, Gaithersburg, MD

ABSTRACT

With the rapid growth of the manufacturing industry, laser-based metal additive manufacturing, such as laser powder bed fusion, has the potential to usher in a revolution. However, its widespread adoption is contingent on the resolution of several challenges. A significant challenge is the uncertainty associated with part consistency when standardized materials are used in additive manufacturing processes. To ensure the quality and reproducibility of AM parts, it is essential to ensure that consistency is maintained. This study delves into an assessment of part-to-part consistency, leveraging a Pyramid learning-based technique that utilizes X-ray computed tomography (XCT) images for four nominally identical parts. Employing machine learning, this approach adopts a hierarchical feature system to enhance model performance. Pyramid Learning not only improves the accuracy of part-to-part consistency scanning but also reduces noise, bolstering overall robustness. The findings showcased the efficacy of pyramid learning in enhancing performance metric when sufficient detail is present. It also provides guidance on locating defects and deformations for the AM parts.

Keywords: Pyramid Learning, Machine Learning, Computer Vision, Additive Manufacturing, X-Ray Computed Tomography, Laser Powder Bed Fusion

1. INTRODUCTION

Machine Learning (ML) has the potential to revolutionize the additive manufacturing (AM) industry by improving the quality, efficiency, and reliability of AM processes [1, 2]. AM, also known as 3D printing, can be made more attractive to manufacturers with ML by enabling the production of new and innovative products [3–5]. X-ray computed tomography (XCT) is a non-destructive imaging technique that can create 3D images of objects. XCT images are created by taking a series of X-ray images of an object from different angles and then using a computer to reconstruct the 3D image from the X-ray images. XCT images are used in various applications, such as manufacturing, medicine, etc. In manufacturing, XCT images can be used to inspect parts for defects or to verify part dimensions. In medicine, XCT images can be used to diagnose diseases, plan surgeries, and monitor the effectiveness of treatments.

Part-to-part consistency is vital in manufacturing as it ensures that parts can be assembled correctly and meet specifications. XCT images are a more efficient and accurate way to verify part-to-part consistency compared to manual inspection methods. By comparing the XCT images of two or more parts, any differences in their dimensions, shapes, or internal structure can be identified. XCT images can improve the quality of manufactured products and reduce the cost of manufacturing.

The purpose of this paper is to present a novel approach for verifying part-to-part consistency using Pyramid Learning. The proposed approach is efficient, accurate, and repeatable. Essentially, image pyramids consist of a collection of images with varying resolutions that are layered on top of each other [6].

XCT was initially used for medical skull modeling in 1990. Later, it was utilized for industrial models and implant production. This paper focuses solely on the industrial applications of these technologies [7, 8]. Obaton et al. used XCT to confirm that additively manufactured parts were geometrically consistent with theoretical specifications. The authors concluded that lattice implants made by selective laser melting improve bone integration [9]. Image quality metrics should be used with caution when assessing lattice structures, as stated by Praniewicz and Fox. These metrics can help evaluate image quality but should be independent of precise dimensional measurements [10].

A real-time Laser Additive Manufacturing (LAM) monitoring system was developed using an IR camera and PID controller. It ensured consistent microstructures with desired cooling rates. This breakthrough can revolutionize LAM, allowing the production of customized parts with tailored microstructures and properties [11]. Zeng et al. proposed a new image inpainting method called PEN-Net. It improves U-Net's structure and includes three components. PEN-Net performed better than the existing methods, generating visually and semantically plausible results [12]. The researchers created the Adaptive FilterBank Pyramid mod-

ule, which combines multiple image processing operators in a single model with continuous parameter tuning. This module is more efficient than the traditional single-operator model while producing similar results [13].

This field is new hence providing a unique opportunity for researchers to contribute significantly to its development. The proposed hierarchical system of features improves part-to-part consistency scanning accuracy, reduces noise, and increases overall method robustness. It also helps locate defects and deformations for AM parts.

The rest of this paper is organized as follows: Section 2 discusses the Materials and Methods, which consist of our data description, processing, and metrics. Analysis and results of the work are given in Section 3. Finally, Section 4 concludes this paper.

2. MATERIALS AND METHODS

2.1 Experiment Setup and Data Description

The experiment was conducted on the Additive Manufacturing Metrology Testbed (AMMT) at the National Institute of Standards and Technology (NIST). AMMT is an open-platform metrology instrument that enables flexible control and measurement of the laser powder bed fusion (L-PBF) [14]. Specific to this experiment, four identical overhang parts were built on an IN625 substrate, $100mm \times 100mm \times 12.5mm$. Powder material was recycled IN625 (this super-alloy is composed mainly of nickel), which was mixed from multiple one-time-used powders. Layer thickness is $20\mu m$. Infilling scan uses $195W$ laser power and $800mm/s$ scan speed. A pre-contour scan uses lower laser power, $100W$, to scan the part outline. To reduce the energy density of this process, the pre-contour scan speed is set to $900mm/s$. More details of the experimental setup and process parameters can be found in the original description file [15].

Figure 1 shows the CAD model of the overhang part with marked key dimensions [16]. As shown, the dashed line divided the part into three $3mm \times 5mm \times 5mm$ regions: 45° constant overhang; cylinder overhang with changing overhang degree; normal support without overhang.

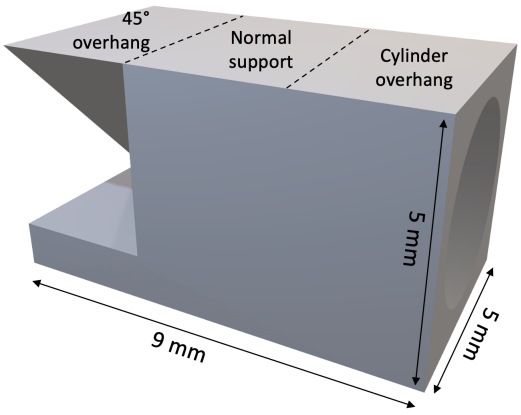

FIGURE 1: OVERHANG PART GEOMETRY

The parts were scanned on a Zeiss Metrotom 800ii. Each part was inserted into a specially designed fixture to locate the parts within the measurement volume repeatably. This was made from EOS PA 2200 (nylon) to reduce the X-ray attenuation of the fixture [17].Also, voxel size is $11.95\mu m \times 11.95\mu m \times 11.95\mu m$. XCT data of each part is provided as a sequence of 16-bit grayscale TIF images. Images are cropped to be $774 pixels \times 440 pixels$. With scaling, this results in an image physical width of $9.25mm \times 5.25mm$.

We divide the part into four zones based on the geometry feature of the part for analysis purposes. As shown in 2, Zone 1 represents the middle region with standard geometry. Zone 2 covers the side with 45° overhang. The cylinder hole region has two symmetric zones, 3 and 4. They have the same geometry in the CAD. However, since these two regions are mostly disconnected during the build, they are formed into two separate zones for comparison.

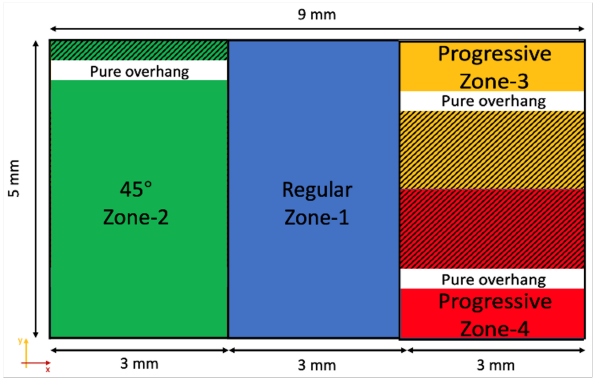

FIGURE 2: ZONE DEFINITION [16]

2.2 Data Processing

It became apparent from analyzing the dataset that different image sets of the parts had distinct visual characteristics. To investigate further, we plotted the grayscale histograms for each part. We normalized the grayscale values across all parts to conduct a precise analysis. After completing a statistical analysis, including the mode, mean, and median, we concluded that the mean grayscale value was the most influential factor for aligning and adjusting the histograms.

Furthermore, After being manufactured, each part went through electrical discharge machining (EDM) to detach it from the building surface. The EDM process aims to cut as close to the surface as possible along the bottom of the part. Since the building design did not need any extra support structures, a portion of the part had to be removed [17]. This caused the parts to have varying heights from what was initially intended. Therefore, the parts' XCT slices or image sequences needed to be aligned. After an analysis, it was discovered that part 4 was removed more extensively from the build plate. As a result, we can compare the other three parts with part 4 to align their XCT image sequences.

For example, the comparison of part 3 and part 4 can be seen in Figure 3. The different colors represent the various number of slices to be removed from the start of the image set of part 3. by observing the Figure, we can see that the colored curves are typically merged, but they diverge around the troughs. For example, we can quickly determine that the blue curve is higher than the others around the first trough, indicating that removing

four layers from part 3 would result in the best similarity. Similar work can also be done for the two other parts. Finally, slices to remove from the start are: Part1: 7, Part2: 6, Part3: 4 slices.

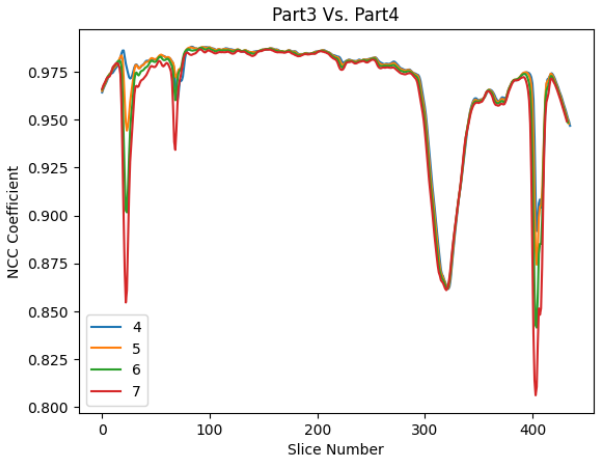

FIGURE 3: DIFFERENT SLICES COUNT REMOVED FROM PART3 ANALYSIS COMPARED TO PART4

After the alignment, the slices associated with the 45-degree overhang region show the best similarity, confirming the alignment. This can be seen in Figure 4.

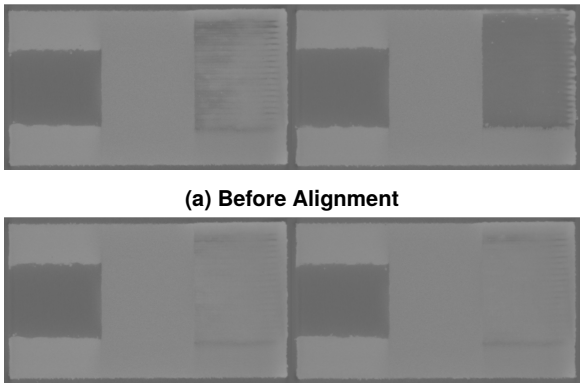

(a) Before Alignment

(b) After Alignment

FIGURE 4: 45 DEGREE OVERHANG REGION OF PARTS 3 AND 4 BEFORE AND AFTER SLICES ALIGNMENT

2.3 Methodology

2.3.1 Normalized Cross-Correlation Coefficient. A normalized cross-correlation coefficient (NCC) was used to analyze the four parts pairwise. This method involves comparing a template image to an input image. The outcome is a correlation map that indicates how well the template corresponds with the input image. The coefficient ranges from 0 to 1, signifying that a score of 1 indicates a perfect match between the images, while 0 indicates complete dissimilarity. Equation 1 defines the normalized cross-correlation coefficient. For each slice, the template image is from one of the parts and the input image is from another part.

$$R(x,y) = \frac{\sum_{x',y'}(T(x',y') - \overline{T})(I(x+x',y+y') - \overline{I})}{\sqrt{\sum_{x',y'}(T(x',y') - \overline{T})^2 \sum_{x',y'}(I(x+x',y+y') - \overline{I})^2}} \quad (1)$$

where

- $R(x,y)$ is the normalized cross-correlation coefficient at pixel (x,y) in the input image.
- $T(x',y')$ is the pixel value at position (x',y') in the template image.
- $I(x+x',y+y')$ is the pixel value at position $(x+x',y+y')$ in the input image.
- $\overline{T}$ is the mean pixel value of the template image.
- $\overline{I}$ is the mean pixel value of the input image.

The NCC metric was used to analyze the parts in a pairwise format. A new method for aggregating information from all parts is presented in the following subsection.

2.3.2 Mean Absolute Difference - Pyramid Learning. The Pyramid Learning technique is an effective tool for analyzing images. It involves starting with the original image at layer 0 and then downsampling it to half the size of the current layer in both height and width. As the pictures are resized into smaller sizes, their similarity typically increases with each subsequent layer. Higher layers show less detail, making the images look more similar. Typically, 4-5 layers are sufficient for this technique.

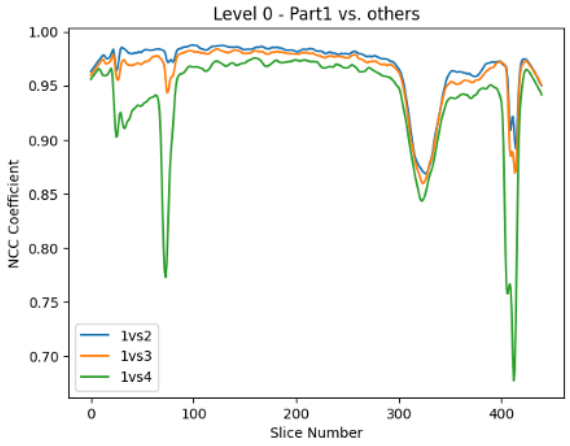

FIGURE 5: NCC COEFFICIENT - PART1 VS. OTHERS

A new metric called "Dissimilarity Score" was introduced for this matter. The general idea is to calculate the mean absolute difference between images as shown in Equation 2. To compute the dissimilarity score, we adopted a four-layer pyramid learning approach. We calculated a score for each layer using Equation 2. Finally, we aggregated the layer scores by averaging them.

$$dst(i,j) = |src1(i,j) - src2(i,j)| \quad (2)$$

where dst is the output image. $src1$ and $src1$ represent the first and the second input image, respectively. i and j are the row and column index.

3. RESULTS AND DISCUSSION

After analyzing with NCC, it was determined that part 4 stands out as the most dissimilar compared to the others. This is because, as stated earlier, Part 4 lost more slices than the other parts during removal from the build plate. Results can be seen in Figure 5. Four noticeable troughs indicate high dissimilarity between the parts in those regions. Upon examining the parts around those slices, it can be inferred that they display specific areas of the parts. The troughs are associated with the following regions:

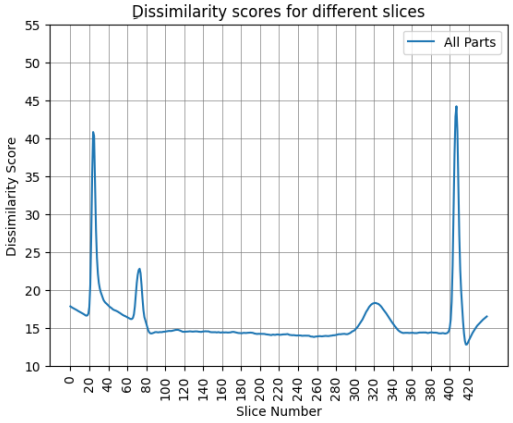

(a) Before slices Alignment

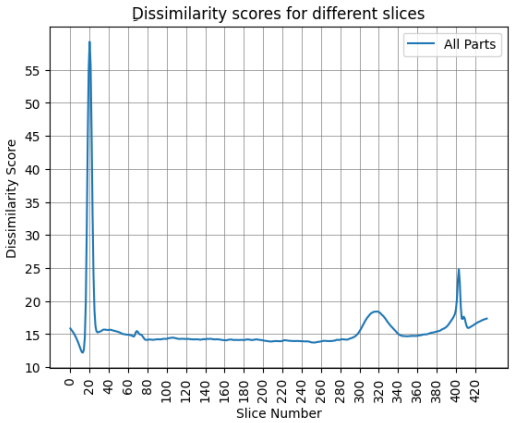

(b) After slices Alignment

FIGURE 6: DISSIMILARITY SCORE WITH PYRAMID LAYERS=4

1) At the beginning, several slices contain the bottom surface of the part. This occurs when the XCT images of the part start to take on a solid form and penetrate deeper into the part.

2) At the start of the cylindrical overhang. This trough can be corrected by aligning the slices, as discussed in 2.2.

3) At the end of the cylindrical overhang, it is customary to observe such a trough due to the randomness caused by the spikes formed from the slices above.

4) Towards the end, several slices contain the top surface. This happens when the XCT images of the part begin to lose their solid form and the part is no longer entirely within the X-ray range.

Overall, the first and fourth troughs hold little significance as they are only present in some of the first and last slices of the parts, and not all of them fall entirely within the X-ray range. Additionally, the XCT images in these slices may not be as consistent as they should be. However, the second and the third troughs are essential and require attention since they are associated with the internal structure of the parts. Additionally, the third peak results from the randomness of spikes from the slices above, so it is natural to have such a trough. After making all the adjustments to the starting slices of the parts, with four layers of the pyramid, the aggregated result is found by taking the average of all pairwise comparisons of the four parts. We can see the improvements in the Dissimilarity Score in Figure 6.

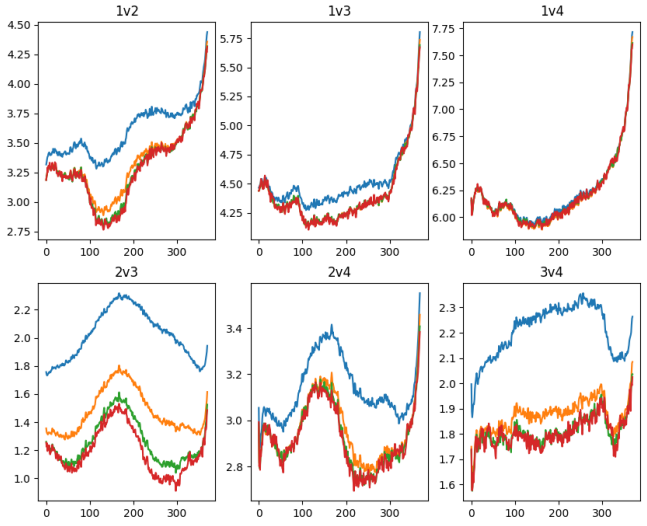

(a) Zone 1 Analysis

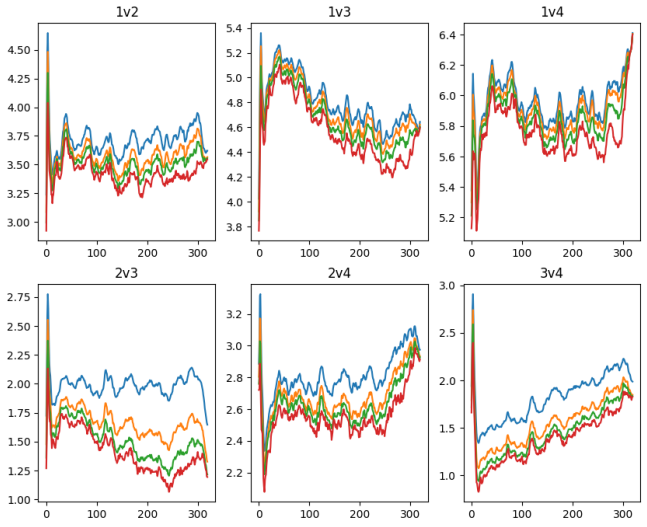

(b) Zone 2 Analysis

FIGURE 7: PYRAMID LEARNING - DISSIMILARITY SCORE

As a final step, we assess the effectiveness of pyramid learning. This approach compares specific zones of different parts instead of analyzing entire images. Zones 2, 3, and 4, which have more detailed information, especially on the edges, can benefit from pyramid learning by reducing the details and resulting in lower dissimilarity scores. However, zone 1 has less detailed information, so pyramid learning is not as helpful. You can observe these results in Figure 7 as the vertical axis shows the Dissimi-

larity Score and the horizontal axis shows different slices of that specific zone. It is worth noting that parts 2 and 4 exhibit halo artifacts in their XCT images (scanning artifacts), which introduce certain details to the images. This explains the discrepancies observed in their corresponding charts compared to parts 1 and 3.

Results of the study are promising and similarities and consistency between parts can be observed. However, in order to confirm these findings and apply them more broadly, further research is required in this field. Additionally, in-situ monitoring data, such as layer camera images and meltpool images, can be included to examine the correlation between these data sources.

4. CONCLUSIONS

Performing an analysis of XCT images is a critical task in additive manufacturing, as it helps verify the printed parts' consistency. To achieve this goal, computer vision algorithms such as pyramid learning can be leveraged, which, in our case, proved effective. There is always some randomness and possible errors in the fabrication and scanning process of the parts. These two factors must be minimized to compare the parts and their qualities more accurately. Pyramid learning can help achieve this objective by removing details, allowing us to investigate the parts with a broader perspective, and ignoring minor errors and randomness. It also guides locating defects and deformations for the AM parts. Future work can be directed to defining standardized metrics to measure AM structure repeatability for part performance.

ACKNOWLEDGMENTS

This work is supported by Department of Commerce, National Institute of Standards and Technology under grant 70NANB22H183.

REFERENCES

[1] Fathizadan, Sepehr, Ju, Feng and Lu, Yan. "Deep representation learning for process variation management in laser powder bed fusion." *Additive Manufacturing* Vol. 42 (2021): p. 101961.

[2] Fathizadan, Sepehr, Ju, Feng, Lu, Yan and Yang, Zhuo. "Deep Spatio-Temporal Anomaly Detection in Laser Powder Bed Fusion." *IEEE Transactions on Automation Science and Engineering* (2023).

[3] Gibson, Ian, Rosen, David W, Stucker, Brent, Khorasani, Mahyar, Rosen, David, Stucker, Brent and Khorasani, Mahyar. *Additive manufacturing technologies*. Vol. 17. Springer (2021).

[4] Kim, Jaehyuk, Yang, Zhuo, Ko, Hyunwoong, Cho, Hyunbo and Lu, Yan. "Deep learning-based data registration of melt-pool-monitoring images for laser powder bed fusion additive manufacturing." *Journal of Manufacturing Systems* Vol. 68 (2023): pp. 117–129.

[5] Ko, Hyunwoong, Yang, Zhuo, Ndiaye, Yande, Witherell, Paul and Lu, Yan. "Machine Learning-driven Process-Structure-Property Analytical Framework for Additive Manufacturing." (2023).

[6] Adelson, Edward H, Anderson, Charles H, Bergen, James R, Burt, Peter J and Ogden, Joan M. "Pyramid methods in image processing." *RCA engineer* Vol. 29 No. 6 (1984): pp. 33–41.

[7] Mankovich, Nicholas J, Cheeseman, Andrew M and Stoker, Noel G. "The display of three-dimensional anatomy with stereolithographic models." *Journal of digital imaging* Vol. 3 (1990): pp. 200–203.

[8] Thompson, Adam, Maskery, Ian and Leach, Richard K. "X-ray computed tomography for additive manufacturing: a review." *Measurement Science and Technology* Vol. 27 No. 7 (2016): p. 072001.

[9] Obaton, AF, Fain, J, Djemaï, M, Meinel, Dietmar, Léonard, Fabien, Mahé, E, Lécuelle, B, Fouchet, JJ and Bruno, Giovanni. "In vivo XCT bone characterization of lattice structured implants fabricated by additive manufacturing." *Heliyon* Vol. 3 No. 8 (2017).

[10] Praniewicz, Maxwell R and Fox, Jason. "Image quality metrics for similarity assessment in the XCT measurement of lattice structures." (2022).

[11] Farshidianfar, Mohammad H, Khajepour, Amir and Gerlich, Adrian. "Real-time control of microstructure in laser additive manufacturing." *The International Journal of Advanced Manufacturing Technology* Vol. 82 (2016): pp. 1173–1186.

[12] Zeng, Yanhong, Fu, Jianlong, Chao, Hongyang and Guo, Baining. "Learning pyramid-context encoder network for high-quality image inpainting." *Proceedings of the IEEE/CVF conference on computer vision and pattern recognition*: pp. 1486–1494. 2019.

[13] Chen, Dongdong, Fan, Qingnan, Liao, Jing, Aviles-Rivero, Angelica, Yuan, Lu, Yu, Nenghai and Hua, Gang. "Controllable image processing via adaptive filterbank pyramid." *IEEE Transactions on Image Processing* Vol. 29 (2020): pp. 8043–8054.

[14] Vlasea, ML et al. "Design, developments, and results from the NIST additive manufacturing metrology testbed (AMMT)." *2016 International Solid Freeform Fabrication Symposium*. 2016. University of Texas at Austin.

[15] Lane, Brandon and Yeung, Ho. "Process monitoring dataset from the additive manufacturing metrology testbed (ammt): Overhang part x4." *Journal of research of the National Institute of Standards and Technology* Vol. 125 (2020): pp. 1–18.

[16] Yang, Zhuo, Adnan, M, Lu, Yan, Cheng, Fan-Tien, Yang, Haw-Ching, Perisic, Milica and Ndiaye, Yande. "Investigating Statistical Correlation Between Multi-Modality In-Situ Monitoring Data for Powder Bed Fusion Additive Manufacturing." *2022 IEEE 18th International Conference on Automation Science and Engineering (CASE)*: pp. 283–290. 2022. IEEE.

[17] Praniewicz, Max, Lane, Brandon, Kim, Felix and Saldana, Christopher. "X-ray Computed Tomography Data of Additive Manufacturing Metrology Testbed (AMMT) Parts:" Overhang Part X4"." *Journal of Research of the National Institute of Standards and Technology* Vol. 125 (2020): pp. 1–9.